



Effect of Al³⁺ ion-substituted Ni–Mg–Co ferrite prepared by sol–gel auto-combustion on lattice structure and magnetic properties

Nanzhaxi Suo¹ · Aimin Sun^{1,2} · Lichao Yu^{1,2} · Zhuo Zuo^{1,2} · Xiqian Zhao^{1,2} · Wei Zhang^{1,2} · Yanchun Zhang^{1,2} · Liqiong Shao^{1,2} · Zhoujia Dang^{1,2}

Received: 3 December 2019 / Accepted: 29 January 2020 / Published online: 12 February 2020
© Springer-Verlag GmbH Germany, part of Springer Nature 2020

Abstract

In this paper, Al³⁺ ion substituted Ni–Mg–Co ferrite nano-magnetic material by sol–gel auto-combustion method. Citric acid is used as a complexing agent, and high-purity nitrate and deionized water are used as raw materials. And the effect of Al³⁺ ion substitution on the structure and magnetic properties of Ni–Mg–Co ferrite nanoparticles was studied. XRD analysis showed that all the samples have the characteristic peak of spinel ferrite. No impurity peaks were found, indicating that the ferrite has a single-phase structure. The average crystallite size was calculated by Debye–Scherrer formula. With the increase of Al³⁺ ion substitution, the average crystallite size decreased from 58.3378 to 51.5249 nm. The structure of Ni–Mg–Co ferrite was characterized by FT-IR. There are two absorption bands ν_1 and ν_2 at 588 cm⁻¹ and 389 cm⁻¹, respectively, which further prove the spinel structure. The morphology of the samples was observed by SEM, and the particle size of the nanoparticles was calculated. The chemical composition of the sample was analyzed by EDS. The elements Ni, Mg, Co, Fe, Al, and O were found in the samples. By VSM analysis, it is found that Al³⁺ ion-substituted Ni–Mg–Co ferrite has ferromagnetic characteristics. With the increase of Al³⁺ ions substitution, the remanent magnetization (Mr), saturation magnetization (Ms), coercive force (Hc), anisotropy constant (K), magnetic moment (μ_B), and Yafet–Kittel angle (α_{YK}) all decreased.

Keywords Sol–gel auto-combustion · Ni–Mg–Co ferrite · Al³⁺ ion substitutes · Nano-magnetic · Materials

1 Introduction

In recent years, scientists have attached great importance to the study of magnetic materials [1]. Nano-magnetic materials are widely used in computer chips, information storage, sensors, optical devices, and devices in the electronic industry [2]. In particular, some semiconductors are also doped with magnetic elements, which make the materials have dual characteristics, such as Fe, Ni magnetic metal elements are doped in SiO₂ [3, 4]. Therefore, the research of magnetic materials is of great significance. The ferrite nano-magnetic materials compared with other materials have higher saturation magnetization and higher coercive force. So the material

has a good research value. Usually in the research of ferrite nano-magnetic materials, we change the magnetism by doping or substituting. In the preparation process of nano-magnetic materials, solid phase reaction, microemulsion method, chemical reaction method, sol–gel method, ball milling method, and coprecipitation method were adopted [5]. In this field, many scholars have also studied. Rahman et al. [6] prepared nano-magnetic materials of Ni–Cu–Zn ferrite substituted by Al³⁺ ions with solid-state method. It found that the average crystallite size, linear density, saturation magnetization, and initial permeability of Ni–Cu–Zn ferrite nano-magnetic materials decrease with the increase of Al³⁺ ion substitution. Qing Lin et al. [7] studied the effect of Al substitution for CoFe₂O₄ ferrite on its structure and magnetic properties. The results show that the lattice constant decreases with the increase of Al³⁺ ions. The coercivity and magnetization increase first and then decrease. Ramkrishna H. Kadam et al. [8] studied the magnetic and electrical properties of Cr³⁺ ions-doped Ni_{0.4}Cu_{0.4}Zn_{0.2}Fe₂O₄ ferrite. It found that the magnetic properties of Ni–Cu–Zn ferrite were affected by the increase of Cr³⁺ ions content. Daniel Fritsch et al. [9, 10] have paid more

✉ Aimin Sun
sunam@nwnu.edu.cn

¹ College of Physics and Electronic Engineering, Northwest Normal University, Lanzhou 730070, China

² Key Laboratory of Atomic and Molecular Physics and Functional Materials of Gansu Province, Lanzhou 730070, China

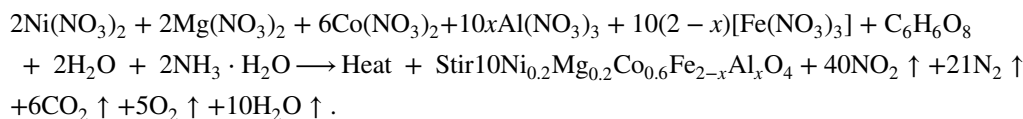
attention to the study of cation distribution and the change of structure and magnetic properties of (A)[B]₂O₄ spinel ferrite. Rajesh Babu et al. [11] studied the nanostructure and magnetic properties of Ni_{0.5}Zn_{0.5}Fe_{2-x}Al_xO₄ ferrite system, the lattice constants and porosity decreased with the increase of Al substitution. Matli Penchal Reddy et al. [12] studied Co-doped Mn-ferrite and found that the lattice constant increased and the saturation magnetization decreased with the increase of Co²⁺ doping amount.

In the present study, Al³⁺ ion substituted Ni–Mg–Co ferrite nano-magnetic material prepared by sol–gel auto-combustion method. We try to adjust the magnetic properties of Ni–Mg–Co ferrite by adjusting wt%. If the suitable Al³⁺ ion is selected to replace Fe³⁺ ion, the lattice structure and magnetic properties of Ni–Mg–Co ferrite may be affected. The purpose of this work is to understand the relationship between the increase of Al³⁺ ion doping content and the magnetic properties of Ni–Mg–Co ferrite nano-magnetic materials. For example, the changes of residual magnetization (MR), saturation magnetization (MS), coercive force (HC), anisotropy constant (k), magnetic moment (μ_B) and Yafet–Kittel angle (α_{YK}) are of great significance.

2 Experimental process

2.1 Preparation materials and methods

In this study, Ni_{0.2}Mg_{0.2}Co_{0.6}Fe_{2-x}Al_xO₄ (x = 0.0, 0.1, 0.2 and 0.3) ferrite nano-magnetic materials were prepared by



sol–gel auto-combustion method. Figure 1 is the flowchart of the sample preparation experiment. The samples were prepared with high-purity citric acid (C₆H₈O₇·H₂O, relative molecular weight 210.14), nickel nitrate [Ni(NO₃)₂·6H₂O, relative molecular weight 290.79], magnesium nitrate [Mg(NO₃)₂·3H₂O, relative molecular weight 256.41], cobalt nitrate [Co(NO₃)₂·6H₂O, relative molecular weight 291.03], aluminium nitrate [Al(NO₃)₃·9H₂O, relative molecular weight 3375.13], and iron nitrate [Fe(NO₃)₃·9H₂O, relative molecular weight 404.00]. By calculating the amount of each sample with a certain molar mass, and then stirring, drying, sintering, annealing etc., Al³⁺ ion was synthesized to substitute Ni–Mg–Co ferrite. The experimental process is divided into two steps. The first, sample preparation; second, sintering to annealing.

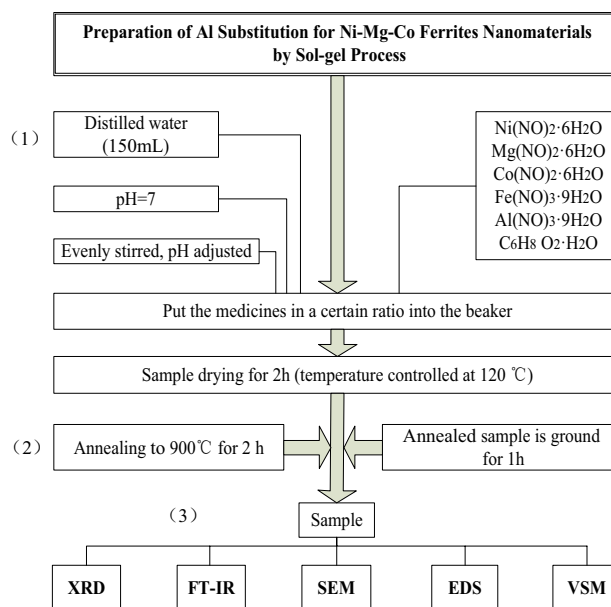


Fig. 1 Preparation of Al substitution for Ni–Mg–Co ferrites nano-magnetic material by sol–gel method

1. Preparing process: The quality of each sample is calculated by a certain molar mass. The measured samples are poured into a clean beaker, and 150 mL distilled water and stirred evenly. The chemical reaction process is as follows:

When ammonium hydroxide was added into the solution after uniform stirring, the solution showed neutrality (pH = 7). The prepared solution is continuously stirred and heated under the operation of the magnetic stirrer (the temperature is controlled at 80°C) until the solution becomes a viscous gel state. Then it is dried in the drying box for 2 h (the temperature is controlled at 120°C).

2. Sintering to annealing process: First, the dried sample is preheated by alcohol lamp. After preheating, continue heating, evaporate all water molecules, and grind the sample into powder state. The powder samples were then annealed in a resistance furnace on 900°C for 2 h. Finally, the samples were ground into powder again and cooled slowly at room temperature.

2.2 Sampling technology

Measuring samples: X-ray diffraction (XRD, Bruch, Germany) was used to measure the crystal plane spacing and half-width; Fourier-transform infrared spectroscopy (FT-IR, WQF-510, China) was used to observe and measure the movement of ν_1 and ν_2 peaks. The morphology of the samples was observed by transmission electron microscopy (TEM, JEM-2010, Japan). Analysis of chemical composition of samples by energy dispersive spectrometer (EDS < SEM >, Jsm-6700F, Japan). Vibration sample magnetometer (VSM, Lakeshore 7304, USA) was used to measure the magnetic properties of samples.

3 Results and discussion

3.1 X-ray diffraction analysis

Ni_{0.2}Mg_{0.2}Co_{0.6}Fe_{2-x}Al_xO₄ ($x=0, 0.1, 0.2$ and 0.3) ferrite nano-magnetic materials were prepared by sol–gel auto-combustion method. Figure 1 is the flowchart of the sample preparation experiment. Figure 2a is an XRD diagram of Al³⁺ ions substituting Ni_{0.2}Mg_{0.2}Co_{0.6}Fe_{2-x}Al_xO₄ ($x=0, 0.1, 0.2$ and 0.3) ferrite sintered to 900°C. Figure 2a shows that the prepared Al³⁺ ion-substituted Ni–Mg–Co ferrite samples have characteristic spinel peaks (111), (220), (311), (222), (400), (422), (511), (440), and (533). It is confirmed that the samples have spinel peak structure. In addition, the spectra show that the diffraction peaks of Al³⁺ ion-substituted Ni–Mg–Co ferrite match well with the characteristic peaks of spinel structure, and it indicated that the prepared samples had a single-phase structure, no impurity peaks were observed in the measured diffraction peaks. Meanwhile, it

showed that all Al³⁺ ions enter the octahedral B-sites of Ni–Mg–Co ferrite, which is consistent with the results in some literatures [13, 14]. Figure 2b shows that the characteristic peaks (311) of samples move toward higher angles. This phenomenon is mainly due to the uniform strain and elastic deformation of the lattice caused by the excitation structure of Al³⁺ ions when Al³⁺ ions (0.53 Å) with smaller ionic radius replace Fe³⁺ ions (0.65 Å) with larger ionic radius. The crystal plane spacing and lattice constants decrease. The lattice of Ni–Mg–Co ferrite will shrink. Average crystallite size is calculated by (FWHM) of XRD diffraction (311) peak and Debye–Scherrer formula. The standard formula is as follows [15]:

$$D = 1.0747\lambda/(\beta \cos \theta). \quad (1)$$

In the formula, ‘ λ ’ is the X-ray diffraction wavelength ($\lambda = 1.5406$), ‘ β ’ is the half-width of the diffraction reflex by XRD. ‘ θ ’ is the diffraction angle of (311) peak. The scanning area of XRD data ranges from 10° to 80°. The lattice constants of samples are calculated by the following formula [15]:

$$a = d\sqrt{h^2 + k^2 + l^2}. \quad (2)$$

Among them ‘ d ’ is the interplanar space and (h, k, l) are the Miller indices. The data in Table 1 are obtained by calculating formulas (1 and 2) above. The data in Table 1 and Fig. 3a show that the lattice constants of the prepared samples decrease with the increase of Al³⁺ ions substitution. The lattice constant decreases from 8.3708 to 8.3251 (Å) (Table 1). This is attributed to the substitution of smaller radius Al³⁺ ions (0.53 Å) [16, 17]. In addition, the average crystallite size of Ni–Mg–Co ferrite decreased from 69.7129

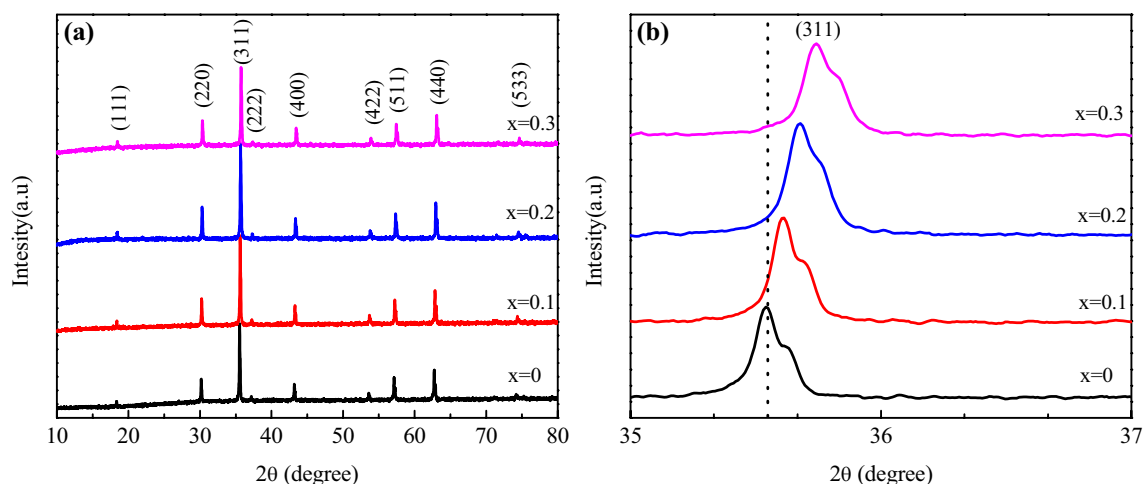


Fig. 2 The XRD pattern of Ni_{0.2}Mg_{0.2}Co_{0.6}Al_xFe_{2-x}O₄ ($x=0.0, 0.1, 0.2,$ and 0.3) nanoferrite along with the figure showing the shifting of the most intense (311) peak

to 61.358 nm with the increase of Al³⁺ ion content. The X-ray density [18–20], is also calculated by the following formula:

$$\rho_x = 8M / (N_A a^3), \tag{3}$$

where, ‘a’, ‘M’ and ‘N_A’ are, respectively, expressed as the lattice constants of the sample, the molecular mass of the sample and the Avogadro constants (N_A = 6.022 × 10²³ mol⁻¹). Considering the shape of the tablet, the following formula is used to calculate the volume density [19]:

$$\rho_b = m / (\pi R^2 l), \tag{4}$$

In the formula, ‘m’, ‘R’ and ‘l’ are the quality, radius and thickness of the tablet, respectively. Considering the effect of the porosity of Ni–Mg–Co ferrite substituted by Al³⁺ ions on the average crystallite size, the porosity of the sample was analyzed. It is well known that the porosity of samples is caused by intergranular pore (Pinter) and intragranular pore (Pintra) [20]. The porosity is equal to the sum of intergranular pore and intragranular pore (P% = Pinter + Pintra). The formula for calculating porosity is as follows [21]:

$$P(\%) = (\rho_x - \rho_b) / \rho_x, \tag{5}$$

Table 1 Parameters obtained from XRD data for Ni_{0.2}Mg_{0.2}Co_{0.6}Al_xFe_{2-x}O₄ (x = 0.0, 0.1, 0.2, and 0.3) nanoferrite particles

Compo- sition ‘x’	Inter planar spacing ‘d’ (Å)	FWHM ‘a’ (Å)	Lattice constant	Average crystallite size ‘D _{XRD} ’ (nm)	Relative error ‘±D _{XRD} ’ × 10 ⁻⁵ (nm)	Volume of unit cell ‘a ³ ’ (Å ³)	Dislocation line den- sity ‘δ’ (10 ⁻⁴ nm ⁻²)
0.0	2.5239	0.143	8.3708	69.7129	6.08	586.54	2.9383
0.1	2.5189	0.146	8.3542	68.2755	8.02	583.06	3.0616
0.2	2.5145	0.168	8.3396	59.3222	0.78	580.01	4.0536
0.3	2.5101	0.162	8.3251	61.5358	8.95	576.99	3.7667

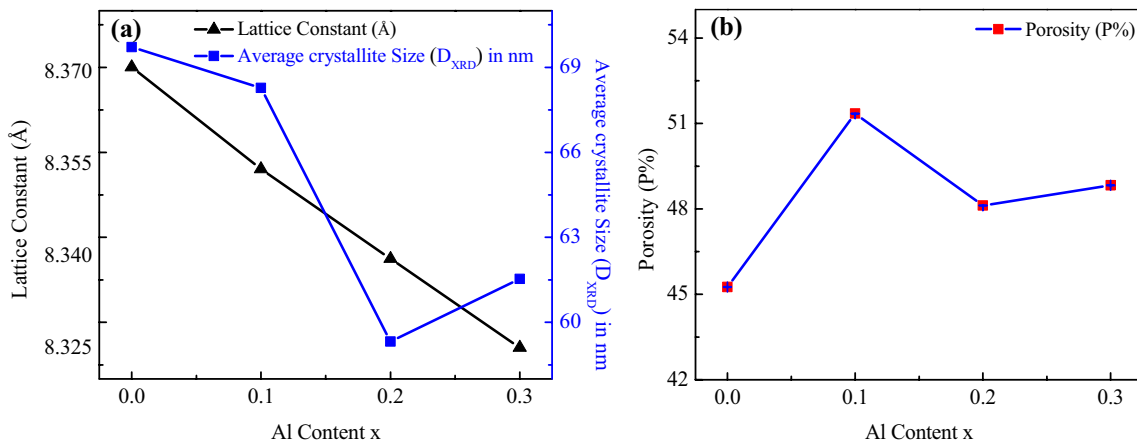


Fig. 3 Variation of latitice constant, average crystallite size, and porosity versus of Al content x

Table 2 Various structural parameters of Ni_{0.2}Mg_{0.2}Co_{0.6}Al_xFe_{2-x}O₄ (x = 0.0, 0.1, 0.2 and 0.3) nanoferrite particles

Composi- tion ‘x’	Molecular weight ‘M’ (g mol ⁻¹)	X-ray density ‘ρ _x ’ (Kg m ⁻³)	Bulk density ‘ρ _b ’ (Kg m ⁻³)	Porosity ‘P’ (%)	Relative error ‘± P(%)’ × 10 ⁻³	Tetrahedral site ‘d _A ’ (Å)	Octahedral site ‘d _B ’ (Å)
0.0	227.6696	6146.5422	3364.65	45.26	9.46	3.4185	2.7912
0.1	224.7838	6105.4469	2970.06	51.35	3.93	3.4116	2.7856
0.2	221.8979	6059.7697	3143.76	48.12	0.80	3.4055	2.7805
0.3	219.0121	6013.0163	3076.59	48.83	4.49	3.3994	2.7756

The dislocation can be calculated by the following formula:

$$\delta = 1/D^2 \quad (6)$$

Formulae (3), (4) and (5) are calculated to obtain the data in Table 2. The data show that the linear density and bulk density decrease with the increase of Al³⁺ ions substitution. This may be due to the fact that the relative atomic mass of Al³⁺ ion (26.98 gm·mol⁻¹) is less than that of Fe³⁺ ion (55.85 gm·mol⁻¹), which leads to the decrease of the lattice constant of the Ni–Mg–Co ferrite. The mass of the sample decreased faster than the cell volume, and the X-ray density decreased. Figure 3b shows that the porosity (*P*%) increases with the increase of Al³⁺ ions substitution. This conclusion is consistent with the results of Al³⁺ substitution of Ni–Zn ferrite by Rajesh Babu et al. [11]. The porosity of Al³⁺ ion substitution Ni–Mg–Co ferrite increases, resulting in the decrease of the average crystallite size. Because the increase of porosity will hinder the movement of crystallite boundaries, thus preventing grain growth [22]. Through the above conclusions, the results of the change of the average crystallite size measured by XRD are more forcefully explained. Similarly, Table 1 data show that the dislocation

lines increase. This indicates that Al³⁺ ions may occupy the lattice gap position in Ni–Mg–Co ferrite crystals. Al³⁺ ion replaces the original basic ion and occupies the grid site in the crystal. The above conclusion can be drawn. In addition, the aberration of crystal structure can activate the accelerated mass transfer of Al³⁺ ions in the crystal when Al³⁺ ions replace Fe³⁺ ions.

3.2 FT-IR spectra analysis

Figure 4a is the Fourier-transform infrared spectra of Ni_{0.2}Mg_{0.2}Co_{0.6}Fe_{2-x}Al_xO₄ ferrite (*x*=0, 0.1, 0.2 and 0.3). The measuring range of the instrument and equipment is 300–4000 cm⁻¹. Two characteristic peaks ν_1 and ν_2 were observed in the spectra. The peaks were 588 cm⁻¹ and 389 cm⁻¹, respectively. These peaks are mainly caused by the tensile vibration of the high-frequency and low-frequency absorption A – site $\leftarrow \text{Zn}^{2+}, \text{Cd}^{2+}, \text{Ga}^{3+}, \text{In}^{3+}, \text{Ge}^{3+}, \text{Mn}^{2+}, \text{Fe}^{3+}, \text{V}^{3+}, \text{Cu}^{1+}, \text{Fe}^{2+}, \text{Mg}^{2+}, \text{Li}^{2+}, \text{Al}^{3+}, \text{Cu}^{2+}, \text{Co}^{2+}, \text{Mn}^{3+}, \text{Ti}^{4+}, \text{Sn}^{3+}, \text{Ni}^{2+}, \text{Cr}^{3+} \rightarrow$ B – site bands passing through tetrahedral A-site and octahedral B-site [23]. In the lattice structure of spinel ferrite, the site of different metal cations is different. Because the chemical bond vibration between

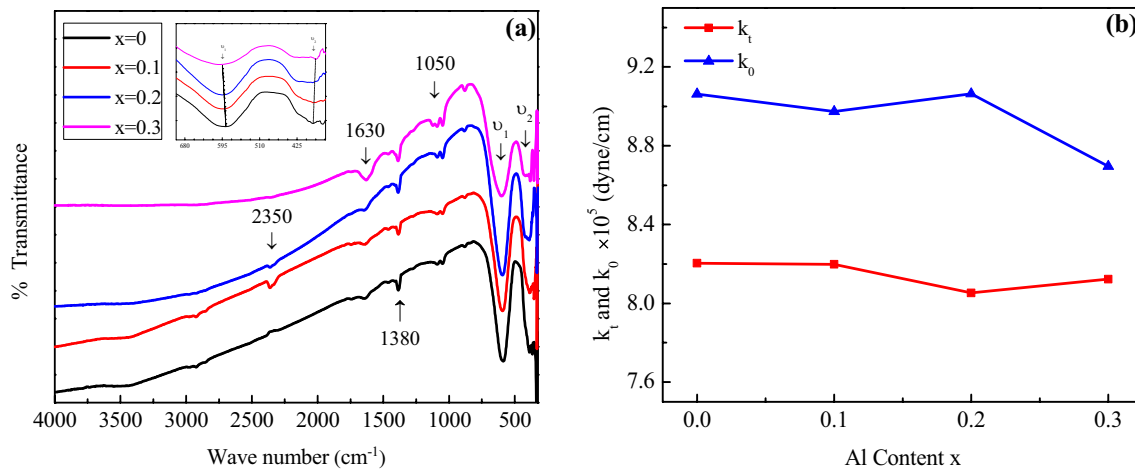


Fig. 4 **a** FT-IR spectra of Ni_{0.2}Mg_{0.2}Co_{0.6}Al_xFe_{2-x}O₄ (*x*=0.0, 0.1, 0.2, and 0.3) nanoferrite system. **b** Variation of force constant k_0 and k_t with Al content *x*

Table 3 Frequency bands ν_1 and ν_2 of the samples of the prepared Ni_{0.2}Mg_{0.2}Co_{0.6}Al_xFe_{2-x}O₄ (*x*=0.0, 0.1, 0.2, and 0.3)

Sample	ν_1 cm ⁻¹	ν_2 cm ⁻¹	Force constant, $\times 10^5$ (dyn cm ⁻¹): ' k_t '	Force constant $\times 10^5$ (dyn cm ⁻¹): ' k_0 '
Ni _{0.2} Mg _{0.2} Co _{0.6} Fe ₂ O ₄	588	389	9.0628	8.2033
Ni _{0.2} Mg _{0.2} Co _{0.6} Fe _{1.9} Al _{0.1} O ₄	593	387	8.9743	8.1985
Ni _{0.2} Mg _{0.2} Co _{0.6} Fe _{1.8} Al _{0.2} O ₄	593	389	9.0644	8.0534
Ni _{0.2} Mg _{0.2} Co _{0.6} Fe _{1.7} Al _{0.3} O ₄	601	381	8.6954	8.1231

A-site metal ion and oxygen atom, chemical bond vibration between B-site metal ion and oxygen atom produces the same absorption peak at high and low frequency [24]. In addition, other absorption peaks of 1050 cm^{-1} , 1380 cm^{-1} , 1630 cm^{-1} , and 2350 cm^{-1} were also found. Characteristic peak ν_1 (588 cm^{-1}) and another characteristic peak ν_2 (389 cm^{-1}) are shown in the Fig. 4. The peak ν_2 is not obvious because the wave number exceeds the instrumental range. The absorption peak of 1050 cm^{-1} is caused by nitrate group, which is similar to that caused by sulfonate group in some references [25]. The absorption peak at 1380 cm^{-1} may be the tensile vibration of carboxylate group and the tetrahedral ferrite complex [26]. The absorption peak at 1630 cm^{-1} may be caused by the stretching vibration of $-\text{OH}$ bond in H_2O molecule [27].

Table 3 shows the position of absorption peaks of $\text{Ni}_{0.2}\text{Mg}_{0.2}\text{Co}_{0.6}\text{Fe}_{2-x}\text{Al}_x\text{O}_4$ ferrite ($x=0, 0.1, 0.2$ and 0.3) substituted by Al^{3+} ion annealed to 900°C . It found that the absorption peak ν_1 shifts to high frequency with the increase of Al^{3+} ion substitution. This is because Fe^{3+} ions with larger radius of ferrite generally occupy the octahedral B-site, and the same is true for Al^{3+} ions in the octahedral B-site. Fe^{3+} ions with larger ion radius are replaced by Al^{3+} ions with smaller ion radius. As a result, the bond lengths of metal cations and oxygen ions ($-\text{O}^{2-}$) at octahedral B-site change, resulting in the difference of frequency bands between ν_1 and ν_2 . Meanwhile, the lattice constant changes due to the distribution in the lower frequency band [28]. It is also mentioned in some literatures that the absorption peak at ν_2 is caused by the imbalance of tetrahedral A-site charge, which may be caused by the movement of oxygen ions. Usually longer bond lengths are formed, but oxygen ions can also form stronger bonds with metal ions [29]. Therefore, the existence of metal cations (M^{2+} or M^{3+}) and oxygen ions ($-\text{O}^{2-}$) in the material was confirmed by FT-IR, which further explained the structure of X-ray diffraction spinel. The force constants at tetrahedral A-site and octahedral B-site are also analyzed. Analysis of metal cations occupying A-site and B-site obtained:

$$(\text{Fe}^{3+})_A[(\text{Ni}_{0.2}^{2+}\text{Mg}_{0.2}^{2+}\text{Co}_{0.6}^{2+})\text{Al}_x^{3+}\text{Fe}_{1-x}^{3+}]_B.$$

XRD analysis shows that the lattice constant decreases with the increase of Al^{3+} ion substitution (Fig. 2a). Meanwhile, we all know that with the decrease of the bond length, the influence frequency increases. Finally, the force constant is calculated by the formula. According to the force constants of tetrahedral A-site and octahedral B-site are the second derivatives of potential energy, the standard formulas are as follows [30]:

$$k_0 = \frac{0.92128M_1V_2^2}{M_1+32}, \quad (7)$$

$$k_t = \frac{0.04416M_2v_1^2}{(u/V) + 3}. \quad (8)$$

Of which:

$$u = \frac{2k_0}{(v_1^2M_1 - 2k_0)}; V = \frac{64.2M_1u}{M_2}.$$

In the formula, ' k_0 ' is the force constant of B-site of octahedron and ' k_t ' is the force constant of A-site of tetrahedron. ν_1 and ν_2 are the frequency bands caused by the bond length vibration between metal cations and oxygen ions at tetrahedral A-site and octahedral B-site, respectively. ' M_1 ' and ' M_2 ' are the molecular mass of tetrahedral site and octahedral site, respectively. Table 3 shows the force constants ' k_t ' and ' k_0 ' with the increase of Al^{3+} ions substitution. Figure 4b and Table 3 show that the force constants ' k_t ' and ' k_0 ' decrease with the increase of Al^{3+} ions substitution. The main reason is that less energy is needed to disconnect the bond length between metal cations and oxygen ions at tetrahedral A-sites and octahedral B-sites. Therefore, the force constant decreases with the increase of Al^{3+} ions. This conclusion is similar to that mentioned in the literature [31]. In the literature, when Co^{2+} ion substituted Li ferrite, the force constant increases with the increase of Co^{2+} ions substitution, and the result of Al^{3+} ion is contrary. Because the radius of Co^{2+} ion (0.74 \AA) is larger than that of Fe^{3+} ion (0.65 \AA) and the radius of Al^{3+} ion (0.53 \AA) is smaller than that of Fe^{3+} ion (0.65 \AA), resulting in the decrease of force constant with the increase of Al^{3+} ions content.

3.3 TEM analysis

The morphology and particle size distribution of Ni–Mg–Co ferrite nanomaterials annealed to 900°C were observed by TEM. Figure 5 shows the TEM image of $\text{Ni}_{0.2}\text{Mg}_{0.2}\text{Co}_{0.6}\text{Fe}_{2-x}\text{Al}_x\text{O}_4$ ($x=0.0$ and $x=0.025$) ferrite. It is observed in TEM that the Ni–Mg–Co ferrite particles are cubic and spherical like. Meanwhile, it is observed that some magnetic nanoparticles adhere to each other and form clusters at high annealing temperature. It is mainly due to the strong interaction between the van der Waals binding energy and the magnetic couple moment between the magnetic nanoparticles [32, 33]. It is also found that the average size of nanoparticles annealed to 900°C in Ni–Mg–Co ferrite ($x=0$ and $x=0.1$) is in the range of $117.2\sim 122.6\text{ nm}$. The shape and size of the nanoparticles are uniform. In addition, Ni–Mg–Co ferrite was characterized by selected area electron diffraction. Figure 6a and b show selected area electron diffraction patterns (SAED) of $x=0$ and $x=0.1$. It is found that the structure of pure samples and samples containing Al^{3+} ions ($x=0$ and $x=0.1$) is similar to that of spinel. It is preliminarily inferred that the Ni–Mg–Co ferrite substituted by Al^{3+} ions has spinel structure. These results correspond well with the XRD data.

Fig. 5 TEM images and particle size distribution diagrams of Al³⁺ ions-substituted Ni_{0.2}Mg_{0.2}Co_{0.6}Al_xFe_{2-x}O₄ nanoferrite particles (annealed to 900 °C): **a, b** represents $x=0.0$ and **c, d** represents $x=0.1$

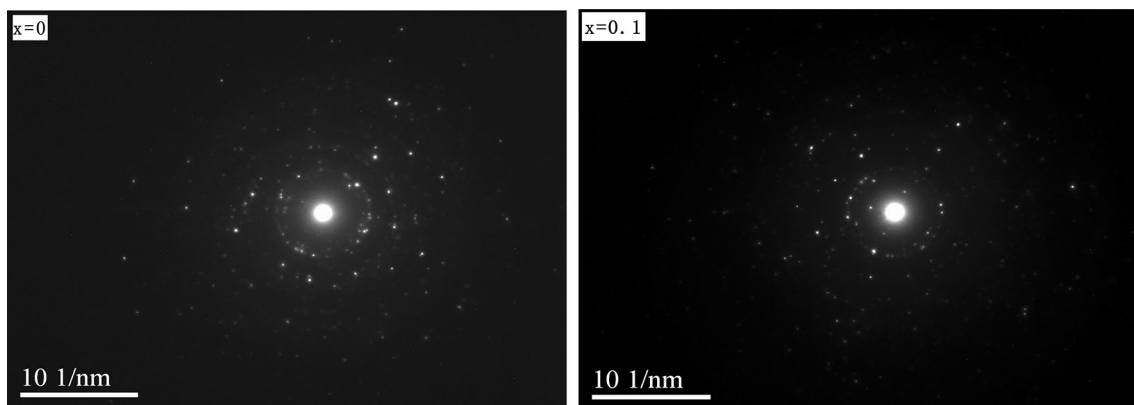
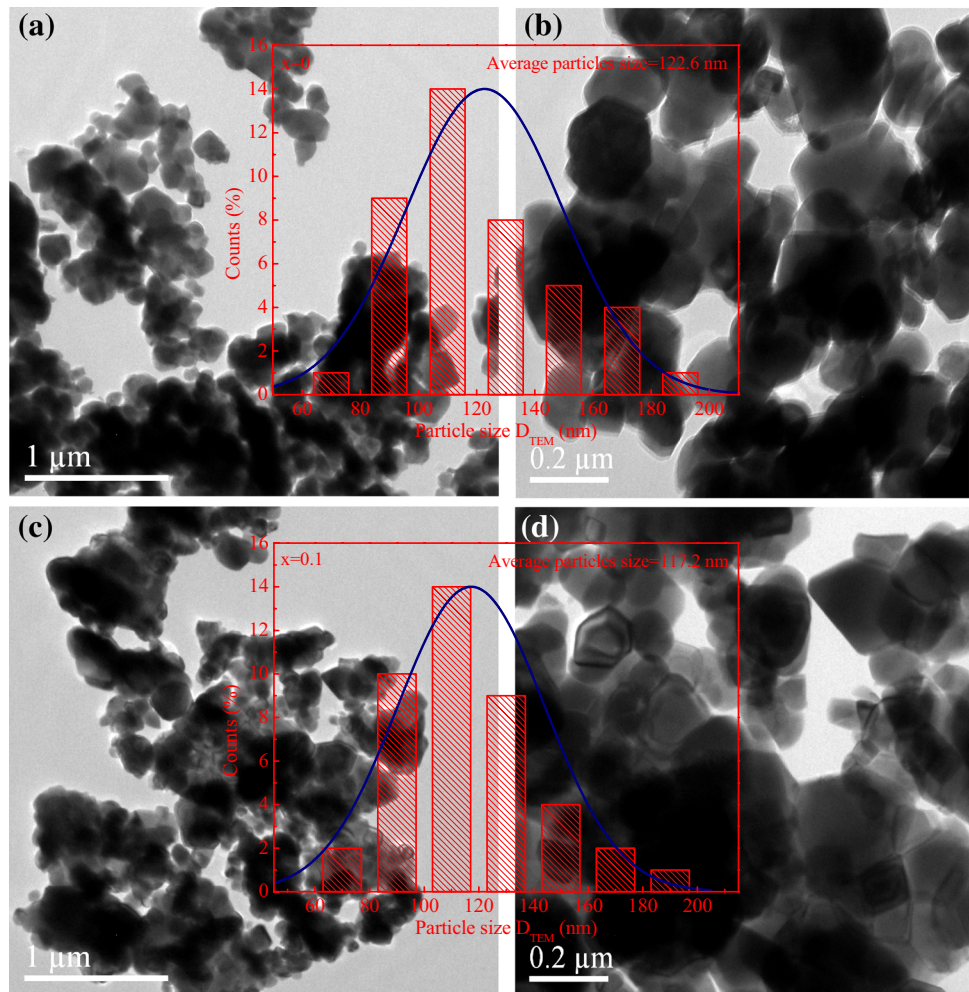


Fig. 6 SAED images of Ni_{0.2}Mg_{0.2}Co_{0.6}Fe_{2-x}Al_xO₄ ($x=0.0$ and 0.1) nanoferrite particles

3.4 Analysis of the chemical composition

The chemical composition of Al³⁺ ion-substituted Ni–Mg–Co ferrite was analyzed by EDS. The chemical formula for the synthesis of nano-magnetic materials is

Ni_{0.2}Mg_{0.2}Co_{0.6}Fe_{2-x}Al_xO₄ ($x=0.0, 0.1, 0.2,$ and 0.3). Figure 7 is a typical EDS spectrum. The presence of Ni, Mg, Co, Fe, Al and O ions plasma in Ni_{0.2}Mg_{0.2}Co_{0.6}Fe_{2-x}Al_xO₄ ($x=0.0, 0.1, 0.2$ and 0.3) nano-magnetic materials was confirmed by EDS spectra. It also found that the X-ray

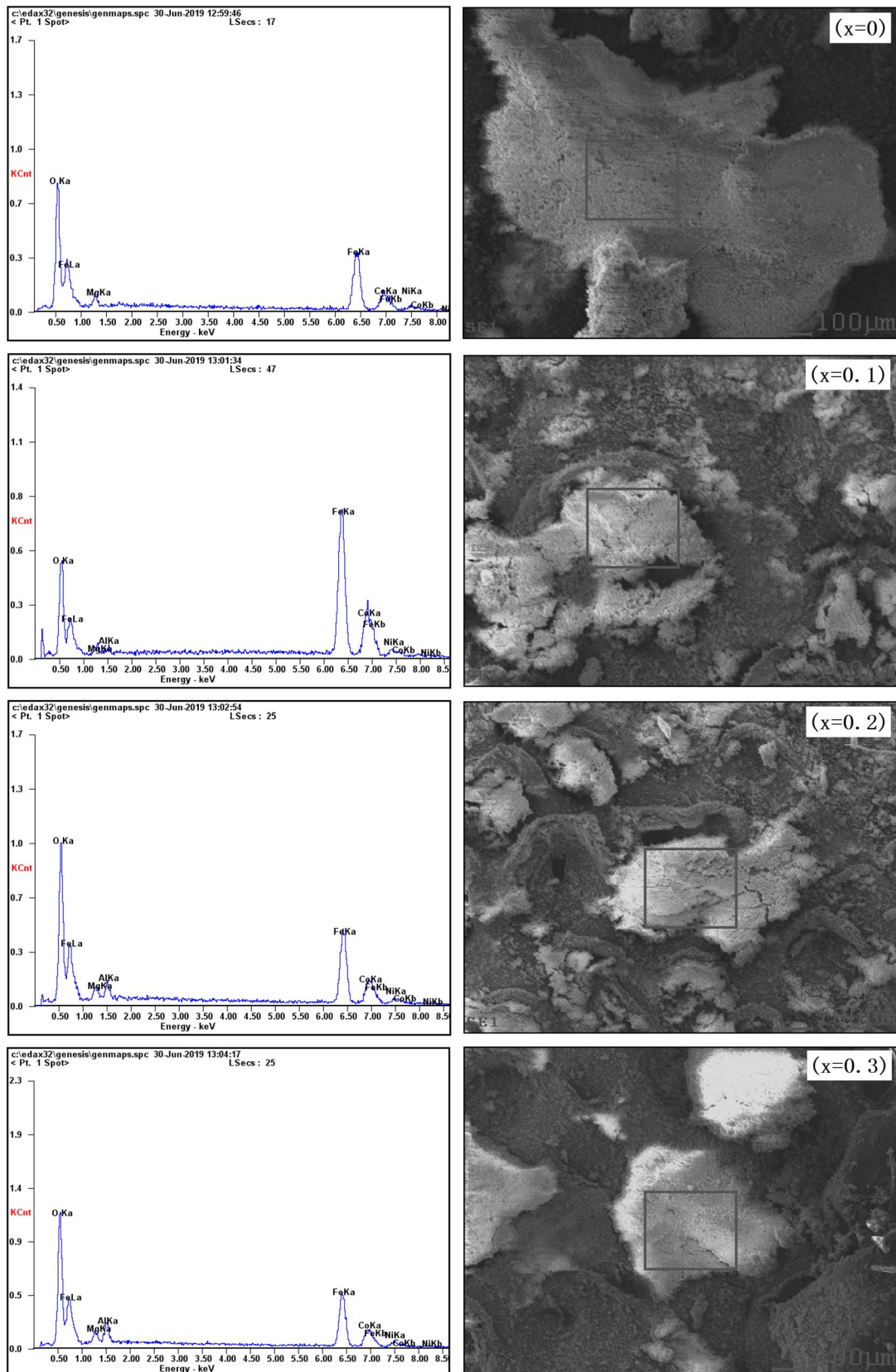
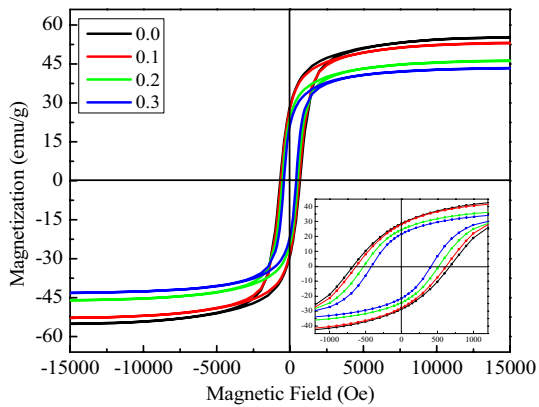


Fig. 7 The EDS diagram of $\text{Ni}_{0.2}\text{Mg}_{0.2}\text{Co}_{0.6}\text{Al}_x\text{Fe}_{2-x}\text{O}_4$ ($x=0.0, 0.1, 0.2,$ and 0.3) nanoferrite sintered on 900°C . The doping amount of each element can be observed in the diagram

Table 4 SThe A-site and B-site magnetic moments and α_{YK} angles of Ni_{0.2}Mg_{0.2}Co_{0.6}Al_xFe_{2-x}O₄ ($x=0.0, 0.1, 0.2$ and 0.3) nanoferrite

Composi- tion 'x'	A-Site	B-Site	M _A	M _B	α_{YK} (degree)
0.0	(Fe ³⁺) _A	(Ni ²⁺ _{0.2} Mg ²⁺ _{0.2} Co ²⁺ _{0.6} Fe ³⁺ ₂) _B	5	12.2	53.540
0.1	(Fe ³⁺) _A	(Ni ²⁺ _{0.2} Mg ²⁺ _{0.2} Co ²⁺ _{0.6} Fe ³⁺ _{1.7} Al ³⁺ _{0.1}) _B	5	11.7	52.454
0.2	(Fe ³⁺) _A	(Ni ²⁺ _{0.2} Mg ²⁺ _{0.2} Co ²⁺ _{0.6} Fe ³⁺ _{1.7} Al ³⁺ _{0.2}) _B	5	11.2	52.423
0.3	(Fe ³⁺) _A	(Ni ²⁺ _{0.2} Mg ²⁺ _{0.2} Co ²⁺ _{0.6} Fe ³⁺ _{1.7} Al ³⁺ _{0.3}) _B	5	10.7	51.301

**Fig. 8** M–H Hysteresis loops of Ni_{0.2}Mg_{0.2}Co_{0.6}Fe_{2-x}Al_xO₄ ($x=0.0, 0.1, 2,$ and 0.3) nanoferrite system

counting (K cnt) increases with the increase of Al³⁺ ions substitution. When ' $x=0$ ', the weight percentage Wt% of Fe³⁺ ions is 52.80, and the atomic substitution At% is 33.63. With the increase of Al³⁺ ion substitution, the weight percentage of Fe³⁺ ion Wt% and atomic hundred substitution At% decrease. When ' $x=0.3$ ', Wt% and At% of Fe³⁺ ions decrease to 45.55 and 27.73, respectively, while Wt% and At% of Al³⁺ ions increase from 0 to 3.96 and 4.99, respectively. It is further explained that a large number of Al³⁺ ions replace Fe³⁺ ions, thus the lattice constant decreases, and the (311) peak of XDR moves to the high angle. Al³⁺ ion substitution has also been successfully realized (Table 4).

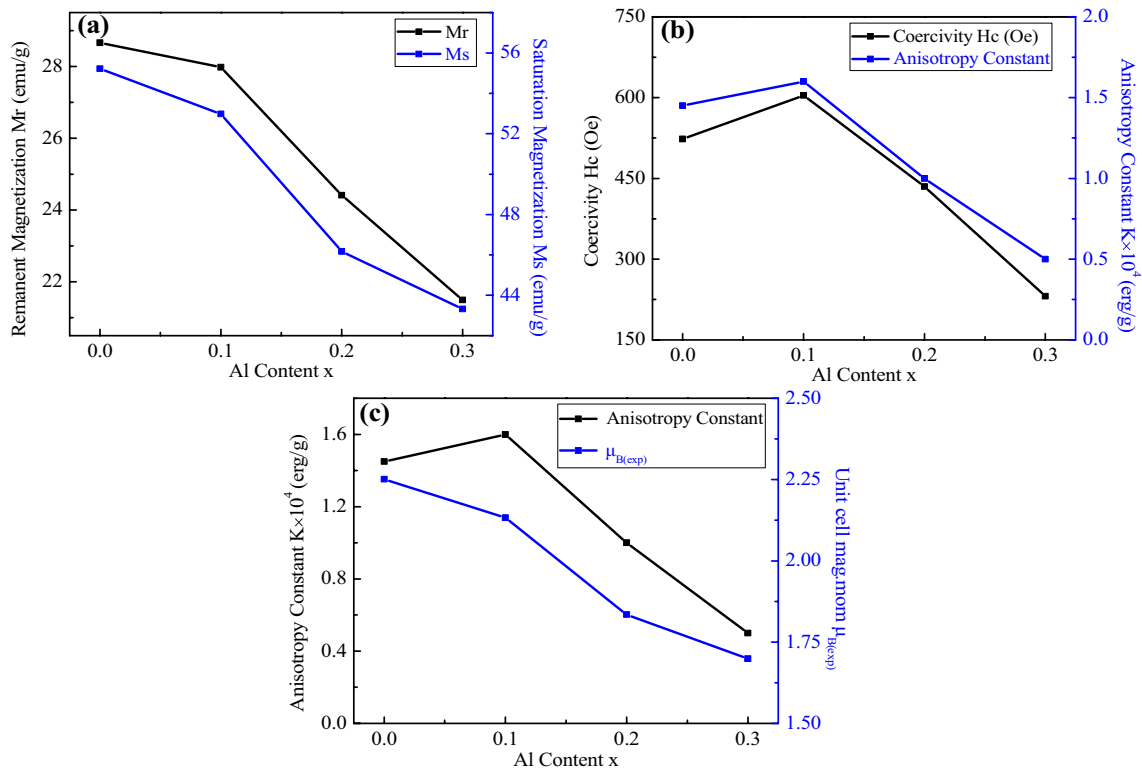
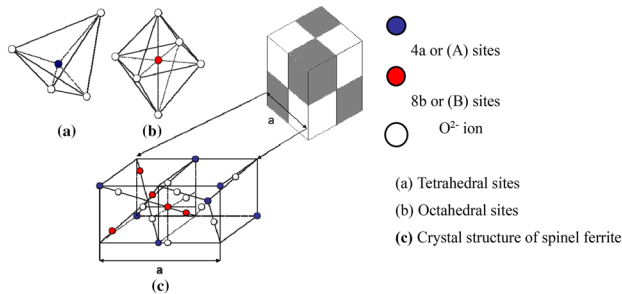
**Fig. 9** Variation of saturation magnetization, remanent magnetization, anisotropy constant, saturation magnetization, and coercivity with Al content x

Table 5 Magnetic parameters of the prepared ferrite samples

Composition 'x'	Remanent magnetization Mr (emu g ⁻¹)	Relative error '±Mr' × 10 ⁻⁵	Saturation magnetization Ms (emu g ⁻¹)	Relative error '±Ms' × 10 ⁻⁵	Coercivity Hc (Oe)	Squareness S (Mr/Ms)
0.0	28.6579	8.25	55.2192	9.82	523.25	0.5189
0.1	27.9792	7.46	52.9792	7.46	604.30	0.5281
0.2	24.4131	5.60	46.1702	1.28	434.79	0.5287
0.3	21.4961	2.55	43.3210	3.32	230.95	0.4962

**Fig. 10** The lattice structure of tetrahedral A-site and octahedral B-site and the distribution of metal cations and oxygen ions

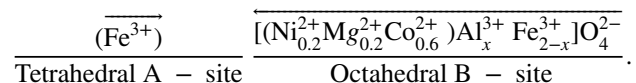
3.5 Magnetic properties

The physical properties of the samples were measured by VSM. Figure 8 shows the hysteresis loops of Ni_{0.2}Mg_{0.2}Co_{0.6}Fe_{2-x}Al_xO₄ ($x=0.0, 0.1, 0.2$ and 0.3) ferrite annealed to 900°C. As shown in Fig. 8, the results show that Al³⁺ ion substitution Ni–Mg–Co ferrite has the characteristics of ferromagnetism, and for ferrite with spinel structure, the main reason affecting their magnetic properties is the type and distribution of cations. Saturation magnetization (Ms), residual magnetization (Mr) and coercivity (Hc) can be observed directly from Fig. 9 (Table 5). In addition, the rectangular ratio (Mr/Ms), dM/dH and 2H_m were measured (shown in Table 5 and Table 6). From Fig. 9a and b and Table 5, it showed that Mr, Ms and Hc, respectively, decrease with the increase of Al³⁺ ions substitution. This may be due to ion superexchange in tetrahedral A-sites and octahedral B-sites in spinel ferrite [34, 35]. However, it is also found from Fig. 9b and Table 5 that when $x=0.1$, the change of Hc has a reverse effect. Hc increased from 523.25 to 604.30 (Oe). It shows that the Hc of $x=0.1$ is larger than that of pure sample. This result is attributed to the uneven magnetization caused by the coupling of strong exchange action in different directions of the surrounding grains when the average crystallite size is the same as the thickness of the domain wall, which ultimately leads to an increase in Hc [36]. Meanwhile, From Table 5, it found that Mr decreases from 28.66 to 21.49 emu g⁻¹; Ms decreases from 55.22 to 43.32 emu g⁻¹; Hc decreases from 523.25 to

Table 6 The values of magnetic moment, magnetic anisotropy, dM/dH, and H_m calculated from M(H) data of Ni_{0.2}Mg_{0.2}Co_{0.6}Al_xFe_{2-x}O₄ ($x=0.0, 0.1, 0.2,$ and 0.3) nanoferrite

Com- position 'x'	Unit cell mag.mom μ _{B(exp.)}	Anisotropy constant K × 10 ⁴ (erg g ⁻¹)	H _m (Oe)	dM/dH (emu g ⁻¹ Oe) × 10 ⁻³	
				H → 0	H → H _m
0.0	2.25	1.45	698.10	23.63	62.32
0.1	2.13	1.60	698.10	24.82	63.19
0.2	1.83	1.00	498.10	23.00	68.20
0.3	1.69	0.50	398.00	26.33	74.59

230.95 Oe. For Co ferrite, Co²⁺ ions mainly fill the octahedral B-sites, and lead to the anisotropy of magnetic lattice through the spin–orbit coupling characteristics of Co²⁺ ions. Well known, Al³⁺ ions mainly occupy octahedron B-sites. With the increase of Al³⁺ ion content, more magnetic cations (Fe³⁺ ions and Co²⁺ ions) in the octahedron B-sites are replaced by Al³⁺ ions. Octahedral B-site Co²⁺ ions are forced to migrate to tetrahedral A-site, while the decrease of Co²⁺ concentration at octahedral B-site leads to the decrease of the anisotropy of magnetic lattice at B-site. Therefore, Mr, Ms and Hc all decreased. It is also stated in some references that the probability of Al³⁺ ion occupying the B-site of octahedron is greater than that of Co²⁺ ion and Fe³⁺ ion. Figure 10 shows the distribution of metal cations and oxygen ions in tetrahedral A-sites and octahedral B-sites. It is a known fact that the relationship between Ms and Mr is well explained by Néel's theory. The spin of the electrons in A-site and B-site eliminates the reverse parallel magnetic moment when the cations in A-site and B-site vibrate [28]. The distribution of metal cations at A-sites and B-sites in Ni–Mg–Co ferrite is as follows:



Similarly, in Ni–Mg–Co ferrite, the Al³⁺ ion occupies the octahedral B-site, and the magnetic moment μ_B of the Al³⁺

ions is '0'. Then a large number of non-magnetic moment Al³⁺ ions replace the Co²⁺ ions on the original octahedral B-sites, which reduces the anisotropic constant of the Co²⁺ ions on the B-sites, resulting in a reduction of the magnetic moment on the octahedral B-sites. The anisotropic constant K is determined by Hc and Ms. The calculation formula is as follows [37]:

$$K = \frac{1}{2} \mu_0 H_c M_s. \quad (9)$$

In the formula, ' μ_0 ' is the permeability in vacuum ($\mu_0 = 1$) and dimensionless in Gauss units (CGS). 'Hc' is the coercivity of the sample and 'Ms' is the saturation magnetization. Figure 9(c) shows that the anisotropy constant decrease with the increase of Al³⁺ ions content. The anisotropy constant of Ni–Mg–Co ferrite is mainly affected by Co²⁺ ion. Because the electron configuration of Co²⁺ ion is 3d⁷ [38], the anisotropy is attributed to the octahedral B-site, resulting in the coupling of frozen orbital angular momentum and spin [39]. Fe³⁺ ion is substituted by Al³⁺ ion, and the spin–orbit coupling at B-site is weakened. Therefore, the anisotropy decreases of Al³⁺ ion-substituted Ni–Mg–Co ferrite. From formula (9), we know that Hc is inversely proportional to Ms, which is consistent with our results. Another observation in Table 5 shows that the coercive force increases sharply with the increase of Al³⁺ ions content. This can be attributed to the large orbital angular momentum anisotropy of Al³⁺ ions. This is the same as the conclusion put forward by Patange et al. [40]. In addition to the inhomogeneous magnetization caused by the superexchange coupling, the relationship between the anisotropy constant and coercive force is explained more forcefully. It is well known that the magnitude of the magnetic moment of the sample is affected by the magnetic moment of the A-site and B-site. The magnetic moment $\mu_B(\text{Cal.})$ is equal to the difference between the magnetic moments of A-sites (M_A) and B-sites (M_B). Its physical expression is [41].

$$\mu_B(\text{Cal}) = M_B - M_A. \quad (10)$$

In addition, the Bohr magnetic moment of Al³⁺ ions substituting for Ni–Mg–Co ferrite can be calculated by the following formula [31]:

$$\mu_B = \frac{M_w \times M_s}{5585}. \quad (11)$$

In the formula, ' M_w ' is the relative atomic mass of the sample, ' M_s ' is the saturation magnetization. The data in Table 5 and Table 6 are obtained from the above formulas (9), (10), and (11). The reason why the anisotropic constant and magnetic moment decrease with the increase of Al³⁺ ions substitution is explained more fully. Table 6 and Fig. 9c shows that the magnetic moment decreases from 2.25 μ_B to 1.69 μ_B . The Hc in the formula (9) is affected by the anisotropy constant K. The

magnetic moments of Ni²⁺, Mg²⁺, Co²⁺, Fe³⁺, and Al³⁺ ions mentioned in some literatures are 2 μ_B , 0 μ_B , 3 μ_B , 5 μ_B and 0 μ_B , respectively. Table 4 shows the changes of magnetic moments at A-sites and B-sites of Ni_{0.2}Mg_{0.2}Co_{0.6}Fe_{2-x}Al_xO₄ ($x = 0, 0.1, 0.2, \text{ and } 0.3$) ferrite doped with Al³⁺ ions. Meanwhile, the magnetic moments of A-sites and B-sites and Yafet–Kittel model are used to calculate the magnetic moments of the samples, which are in unit $\mu_B(\text{Cal})$ [42, 43]. The calculation formula is as follows:

$$\mu_{B(\text{exp})} = M_B \cos \alpha_{YK} - M_A. \quad (12)$$

So Y–K angle α_{YK} can be written as:

$$\cos \alpha_{YK} = \frac{\mu_{B(\text{exp})} + M_A}{M_B}. \quad (13)$$

The magnetic moments of A-sites and B-sites [44], namely:

$$(Fe^{3+})_A [Ni_{0.2}^{2+} Mg_{0.2}^{2+} Co_{0.6}^{2+} Al_x^{3+} Fe_{2-x}^{3+} O_4^{2-}]_B,$$

$$M_A = 1 \times 5 \mu_B,$$

$$M_B = [0.2 \times 2 + 0.2 \times 0 + 0.6 \times 3 + (2 - x) \times 5 + x \times 0] \mu_B, \\ = (12.2 - 5x) \mu_B.$$

The Y–K angle α_{YK} obtained from the above formulas (12), (13) and the above theoretical calculations. It is shown in Table 4, the magnetic stability and magnetic recording of Ni_{0.2}Mg_{0.2}Co_{0.6}Fe_{2-x}Al_xO₄ ($x = 0, 0.1, 0.2 \text{ and } 0.3$) ferrite nano-magnetic materials can also be described by the rectangular ratio (S) and the switching field distribution (SFD).

$$\left. \frac{dM}{dH} \right| = \frac{M_r}{H_c (1 - S^*)}, \quad (14)$$

$$SDF = \frac{\Delta H}{H_c}. \quad (15)$$

The data in Table 6 and Fig. 11. show that the width of dM/dH curve decreases and the 2Hm peak increases with the increase of Al³⁺ ions substitution. The results show that there are very few stable particles in the sample and the rewriting performance is good. The stable particles retain the original direction of magnetization when the magnetic record is not easily written to the field reversal. It is also found that the peak value of 2Hm is symmetrical at $H = 0$. The values of $H \rightarrow H_m$ at $x = 0, 0.1, 0.2 \text{ and } 0.3$ are 62.32 $\times 10^{-3}$ emu g⁻¹ Oe, 63.19 $\times 10^{-3}$ emu g⁻¹ Oe, 68.20 $\times 10^{-3}$ emu g⁻¹ Oe and 74.59 $\times 10^{-3}$ emu g⁻¹ Oe, respectively. Compared with pure samples, a large number of unstable regions appear in the superparamagnetic region with the increase of Al³⁺ ion substitution. This may be largely influenced by the structure of nano-magnetic lattices. However, from the magnetic record rewriting energy, the performance of the sample is enhanced.

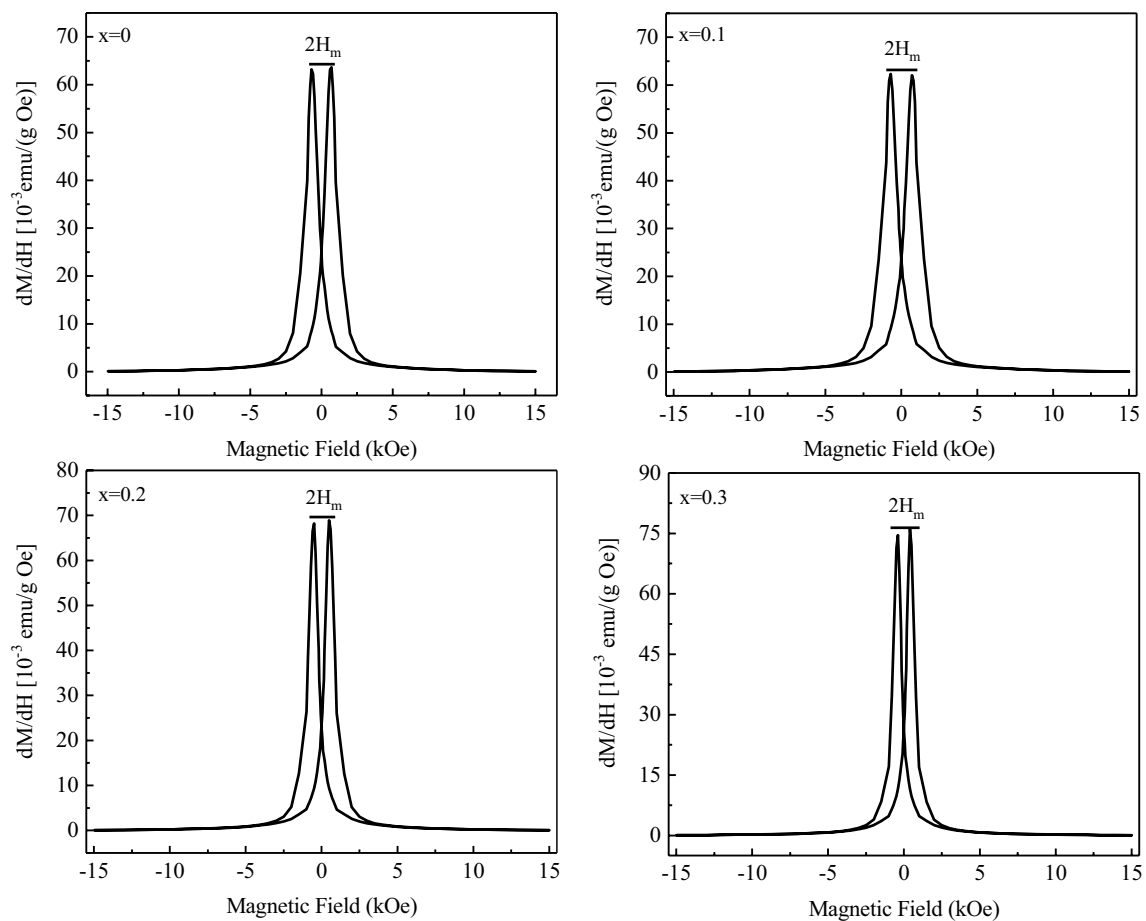


Fig. 11 Field dependence of dM/dH of different samples. $2H_m$ measures the magnetic field that separates two peaks

4 Conclusions

Al^{3+} -ion-substituted Ni–Mg–Co ferrite nanomaterials were prepared by sol–gel auto-combustion method:

The XRD diffractogram show that all Al^{3+} ion-substituted Ni–Mg–Co ferrite samples have single-phase spinel structure. It was also found that the peak (311) shifted to the higher angle, indicating that the average crystallite size decreased with the increase of Al^{3+} ions substitution. The average crystallite size was calculated by Debye–Scheller formula. The average crystallite size decreased from 69.7129 to 61.5358 nm. The spinel structure of Al^{3+} ion-substituted Ni–Mg–Co ferrite was confirmed by Fourier-transform infrared spectroscopy (FT-IR). It is also found that the absorption peaks ν_1 at 588 cm^{-1} and ν_2 at 389 cm^{-1} move in high-frequency direction. The force constants k_0 and k_t caused by two bond lengths are calculated by two absorption peaks. It is found that the force constants decrease with the increase of Al^{3+} ion substitution. The morphology of the samples was observed by scanning electron microscopy, and the average

particle size was calculated. The average particle size ranged from 117.2 to 122.6 nm. The chemical composition of Al^{3+} ion-substituted Ni–Mg–Co ferrite was analyzed by EDS. It was explained that Al^{3+} ions were successfully doped into Ni–Mg–Co ferrite. In addition, Ni, Mg, Co, Fe, Al and O were found in the samples. The ferromagnetic properties of Ni–Mg–Co ferrite substituted by Al^{3+} ions were confirmed by VSM measurements. By VSM analyzing, with the increase of Al^{3+} ion content, the M_r decreases from 28.66 to 21.49 emu g^{-1} , the M_s decreases from 55.22 to 43.32 emu g^{-1} , the H_c decreases from 604.30 to 230.95 Oe, the anisotropic constant (K) decreases from 1.45×10^4 to 0.5×10^4 erg g^{-1} , magnetic moment (μ_B) increases from 2.25 to 1.69, the α_{YK} decrease from 53.540 (degree) to 51.301 (degree).

Compliance with ethical standards

Conflict of interest The author states that there is no conflict of interest with other institutions (financial or non-financial, directly or indirectly related to work, in all scientific fields).

Ethical standards The author states that the manuscript complies with the ethical rules applicable to the journal.

References

- G.V. Williams, T. Prakash, J. Kennedy, S.V. Chong, S. Rubanov, J. Magn. Mater. **229**, 460 (2018)
- J. Kennedy, J. Leveueur, G.V.M. Williams, D.R.G. Mitchell, A. Markwitz, Nanotechnology **115602**, 22 (2011)
- Y. Wang, L.-T. Tseng, P.P. Murmu, N. Bao, J. Kennedy, M. Ionesc, J. Ding, K. Suzuki, S. Li, J. Yi, Mater. Des. **77**, 121 (2017)
- T. Prakash, G.V. Williams, J. Kennedy, S. Rubanov, J. Alloy Comp. **255**, 667 (2016)
- M.M. Eltabey, K.M. El-Shokrofy, S.A. Gharbia et al., J. Alloys Compd. **2473**, 509 (2011)
- K.R. Rahman, F.-U.-Z. Chowdhury, M.N.I. Khan, Result Phys. **354**, 7 (2017)
- Q. Lin, Y. He, J. Xu, J. Lin, Z. Guo, F. Yang, Nanomaterials **2**, 750 (2018)
- R.H. Kadam, A. Karim, A.B. Kadam, A.S. Gaikwad, S.E. Shirsath et al., Int. Nano. Lett. **2**, 28 (2012)
- D. Fritsch, Phys. Rev. B. **86**, 014406 (2012)
- V. Stevanovic, M. Avezac, A. Zunger, Phys. Rev. Lett. **105**, 075501 (2010)
- B.R. Babu, M.S.R. Prasad, K.V. Ramesh, Y. Purushotham, Mater. Chem. Phys. **585**, 148 (2014)
- M.P. Reddy, X. Zhou, A.Y.S. Dua, Q. Huang, A.M.A. Mohamed, Super Micro. **233**, 81 (2015)
- S. Singhal, S.K. Barthwal, K. Chandra, J. Magn. Mater. **233**, 306 (2006)
- K.P. Chae, J.-G. Lee, H.S. Kweon, Y.B. Lee, Phys. Status Solidi **1883**, 201 (2004)
- A.B. Gadkaria, T.J. Shindeb, P.N. Vasambekar, Mater. Chem. Phys. **505**, 114 (2009)
- A.T. Raghavreender, K.M. Jadhav, Indian academy of sciences. Bull. Mater. Sci. **575**, 32 (2009)
- I. Ahmada, T. Abbasa, M.U. Islama, A. Maqsood, Ceram. Int. **6735**, 39 (2013)
- J. Smit, H.P.J. Wijn, *Ferrite* (John Wiley, New York, 1959)
- S.G. Gawas, U.B. Gawas, V.M.S. Verenkar, M.M. Kothawale, R. Pednekar, J Super Nov. Magn. **1447**, 30 (2017)
- N. Rezlescu, E. Rezlescu, C. Pasnicu, M.L. Craus, J. Phys. Condens. Matter. **5707**, 6 (1994)
- H.E. Hassan, T. Sharshar, M.M. Hessien, O.M. Hemeda, Nucl. Instrum. Methods Phys. Res. B. **72**, 304 (2013)
- Y. Matsuo, K. Ono, M. Ishikura, I. Sasaki, IEEE Trans. **3751**, 33 (1997)
- Q.M. Wei, J.B. Li, Y.J. Chen, J. Mater. Sci. **5115**, 36 (2001)
- X.G. Pan, A.M. Sun, Y.Q. Han, Moder. Phys. Lett. B **32**, 1850321 (2018)
- S. Maensiri, C. Masingboon, B. Boonchomb, S. Seraphinc, Scr. Mater. **797**, 56 (2007)
- S. Rana, J. Phili, B. Raj, Mate. Chem. Phys. **264**, 124 (2010)
- Z. Mosleh, P. Kamelin, M. Ranjbar, H. Salamati, Ceram. Int. **7279**, 140 (2014)
- C.K.Y. Yafet, Phys. Rev. **290**, 87 (1958)
- A. Ali, Ati, Zulkafli Othaman, Alireza Samavati, Fatemeh Yaghoubi Doust. J. Mol. Struct. **136**, 1058 (2014)
- V.S. Sawant, A.A. Bagade, S.V. Mohite, K.Y. Rajpure, Phys. B **39**, 451 (2014)
- S.R. Sawant, S.S. Suryavanshi, Curr. Sci. **644**, 57 (1998)
- F. Köseoğlu, F. Alan, M. Tan, Resul Yilgin and Mustafa öztürk. Ceram. Int. **3625**, 38 (2012)
- T. Prakash, G.V.M. Williams, J. Kennedy, S. Rubanov, J. Appl. Phys. **120**, 123905 (2016)
- A.A. Kadam, K.Y. Rajpure, J. Mater. Sci. **10484**, 27 (2016)
- J. Wang, C. Zeng, Z. Peng, Q. Chen, Phys. B **124**, 349 (2004)
- G. Herzer, IEEE Trans. Magn. **1397**, 20 (1990)
- J.M.D. Coey, *Rare-earth iron permanent magnets* (Oxford University Press, Oxford, 1996)
- I. Sharififi, S.H. Nanostructural, J. Magn. Mater. **2397**, 324 (2012)
- F. Gözüak, Y. Köseoglu, A. Baykal, H.J. Kavas, Magn. Mater. **2170**, 321 (2009)
- S.M. Patange, S.E. Shirsath, B.G. Toksha, S.S. Jadhav, K.M. Jadhav, J. Appl. Phys. **023914**, 106 (2009)
- S.S. Jadhav, S.E. Shirsath, S.M. Patange, K.M. Jadhav, J. Appl. Phys. **2**, 108 (2010)
- S.S. Jadhav, S.E. Shirsath, S.M. Patange, J. Appl. Phys. **381**, 108 (2010)
- S.A. Mazen, N.I. Abu-Elsaad, J. Magn. Mater. **3366**, 324 (2012)
- M.M. Eltabe, K.M. El-Shokrofy, S.A. Gharbia, J. Alloy Comp. **2473**, 509 (2011)

Publisher's Note Springer Nature remains neutral with regard to jurisdictional claims in published maps and institutional affiliations.